


Article

Optimizing Contact Force on an Apple Picking Robot End-Effector

Hongwei Zhang , Wei Ji *, Bo Xu and Xiaowei Yu

School of Electrical and Information Engineering, Jiangsu University, Zhenjiang 212013, China; zhanghongwei991016@163.com (H.Z.); xubo@ujs.edu.cn (B.X.); 18879209223@163.com (X.Y.)

* Correspondence: jiwei@ujs.edu.cn

Abstract: The quality of apple picking affects the sales of apples, and the grasping force of the end effector of an apple picking robot is very important for apple picking. It is easy to cause apple damage due to excessive contact force, or when the contact force is too small to grasp the apple. However, the current research lacks an analysis of the minimum stable grasping force of apples. Therefore, in order to realize the stable grasping of apples by the end-effector of a picking robot and reduce fruit damage, this study first analyzes the grasping stability of the end-effector based on the force closure theory, and comprehensively considers the force closure constraints, nonlinear friction cone constraints and the introduction of torque constraints. Next, the constraint conditions are processed using an obstacle function, and a penalty factor is introduced to construct an optimization model of the contact force distribution of the end-effector. Then, the improved Newton method is used to grasp and solve the contact force distribution model. Under the premise of selecting the penalty factor, the optimal contact force of grasping an apple is determined using a method of numerical example simulation analysis, and the validity of the solution is verified. In order to verify the reliability of the contact force distribution optimization model, the practical significance of the method for apple grasping is verified in an actual grasping experiment. The actual experiment shows that the method can provide the minimum stable grasping force to the end-effector to achieve stable grasping.

Keywords: apple picking robot; end-effector; grasping stability; optimization of contact force; constraints



Citation: Zhang, H.; Ji, W.; Xu, B.; Yu, X. Optimizing Contact Force on an Apple Picking Robot End-Effector. *Agriculture* **2024**, *14*, 996. <https://doi.org/10.3390/agriculture14070996>

Academic Editors: Mustafa Ucgul and Massimo Cecchini

Received: 14 May 2024

Revised: 18 June 2024

Accepted: 24 June 2024

Published: 25 June 2024



Copyright: © 2024 by the authors. Licensee MDPI, Basel, Switzerland. This article is an open access article distributed under the terms and conditions of the Creative Commons Attribution (CC BY) license (<https://creativecommons.org/licenses/by/4.0/>).

1. Introduction

The apple picking robot hardware consists mostly of a chassis, manipulator, end-effector, and camera [1,2]. The end-effector, in particular, has a crucial function as it is responsible for the separation and picking of apples [3]. Hence, it is crucial to investigate the optimization of contact force distribution throughout the apple picking process.

Researchers have conducted numerous studies on the ways to optimize grasping stability and the contact force of items. Chen et al. [4] constructed regularization optimization problems using obstacle functions, gave a comprehensive representation of objective functions with different dimensions, and introduced a penalty factor to form an augmented optimization objective function. For a specific operation task, a more compact, stable or relaxed flexible grasping scheme can be obtained by adjusting the penalty factor. James et al. [5] employed sliding detection to guarantee the stability of the gripping procedure. The reliability of the detection method in unstructured situations was confirmed by employing the support vector product to identify sliding and test various sliding scenes. In their study, Mavrakis et al. [6] introduced a novel approach for assessing the stability of robot grasping. This method involves determining the intrinsic stiffness matrix of a two-finger grasp and using it to establish a stability metric. The metric takes into account many factors such as local contact curvature, material properties, contact force, and target mass. Xu et al. [7] proposed a fast force-closure grasp synthesis (FFCGS) method for an anthropomorphic hand to efficiently grasp unknown objects. The outcomes of this study

have great significance in promoting the motion planning of robot hand-arm systems and upper-limb prostheses. Li et al. [8] expanded upon the existing grasping stability theory for rigid items to examine the stability of grabbing semi-ripened tomatoes. They determined that curved fingers are better suited for securely holding tomatoes compared to disc-shaped fingers.

While numerous scholars have examined the impact of different factors on grasping stability, it is important to optimize the contact force applied to the fruit tissue to ensure stability without causing damage. Buss et al. [9] introduced a recursive optimization technique that is well-suited for dynamic situations. The purpose of this method is to determine an appropriate set of internal grasping forces that can accomplish both grasping stability and minimize grasping energy. In their study, Li et al. [10] aimed to identify the contact point location during dynamic operations that fulfills the force closure criterion based on the equivalency between the friction point constraint and the positive definite symmetric matrix found by Buss, they employed an iterative optimization algorithm to maximize the contact force of the jaw and determine the appropriate clamping force. In order to facilitate a systematic and precise examination of the force closure of MCDRMs with a cable routing design, Liang et al. [11] presented a novel force-closure analysis approach for MCDRMs that takes into account both cable coupling and friction effects. Nonlinear contact force distribution issues are defined by Liu et al. [12] as smooth manifold optimization problems that relate to a positive definite matrix that is linearly limited. The contact force is optimized using a quadratic index gradient flow method that is based on a low-dimensional description matrix. Li et al. [13] introduced a technique for evaluating the stability of envelope grasping using geometric analysis. They also developed an optimal method for planning envelope grasps, which involves determining the necessary deployment length of the DRH and ensuring a secure grip.

The above research has basically considered various constraints of force closure and optimized the grasping force optimization algorithm to a certain extent, but the applications for agricultural picking robots is relatively few. This study will conduct further research on the basis of these studies and introduce torque constraints on the premise of synthesizing the above constraints. At the same time, this study will consider optimizing the grasping force of the grasping model under new constraints, and apply the idea of the penalty function [14] to the apple picking robot in order to achieve higher computational efficiency and finally achieve acquisition of the minimum stable grasping force of the apple picking robot, which is also the focus of this research. The main contributions of this research are as follows:

- (1) The grasping stability of the end-effector will be analyzed based on the force closure theory for an apple picking robot, and the optimal model of the end-effector contact force distribution will be constructed by introducing a penalty factor;
- (2) The improved Newton method will be applied to the contact force distribution model, and the high computational efficiency of this method will be analyzed using numerical simulation;
- (3) The actual grasping experiment will further verify that this method can achieve the minimum stable grasping force of an apple picking robot and realize the stable grasping of the apple.

The rest of the paper is organized as follows. Section 2 introduces the stability analysis of the end-effector based on the force closure theory, establishes the optimization model of force distribution, and introduces how to solve it. Section 3 details the numerical example calculation, simulation and experimental analysis and discussion. Section 4 summarizes the full paper.

2. Materials and Methods

The contact force and joint velocity vector in the operating space represent the translation of the generalized contact force and velocity screw of each finger in the operating space. This can be manifested as the coordination among numerous fingers [15]. The friction point

contact model is used as the grasping model for force closure analysis as the end-effector used in this paper is a rigid device [16], which has three fingers and will be introduced in detail in the later experimental equipment introduction.

2.1. Friction Cone Constraint and Analysis

The contact force of the end-effector grasping the apple f_i can be separated into a unidirectional parameter f_{iz} and two intersecting parameters f_{ix} and f_{iy} , as seen in Figure 1.

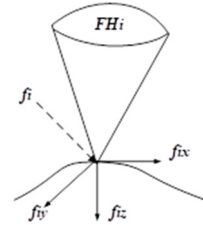


Figure 1. Schematic diagram of contact force components.

To avoid the apple from sliding, the contact force components must satisfy the constraint condition [17]. The constraint condition is shown in Equation (1).

$$\|(f_{ix}, f_{iy})\|_2 = \sqrt{(f_{ix}^2 + f_{iy}^2)} \leq \mu_i f_{iz}, \quad i = 1, 2 \dots n \tag{1}$$

Here, μ_i represents the friction coefficient.

The friction constraint condition at the contact point i of the apple picking robot end-effector can be mathematically represented as a second-order cone, as illustrated in Equation (2).

$$FH_i = \left\{ f_i \in R^3 \mid \frac{1}{\mu_i} \sqrt{(f_{ix}^2 + f_{iy}^2)} \leq f_{iz} \right\}, \quad i = 1, 2 \dots n \tag{2}$$

Here, FH_i represents the friction constraint at contact point i of the end-effector.

The above friction cone constraint conditions can be made equivalent using a linear matrix inequality (LMI), that is, $f_i \in FH_i$ can be expressed as the form shown in Equation (3).

$$\begin{bmatrix} \mu_i f_{iz} & 0 & f_{ix} \\ 0 & \mu_i f_{iz} & f_{iy} \\ f_{ix} & f_{iy} & \mu_i f_{iz} \end{bmatrix} \geq 0 \tag{3}$$

2.2. Force Closure Constraint and Analysis

To accurately represent the overall impact of the contact force, it is essential to convert the contact force f_i of each fingertip of the end-effector into the coordinate system where the apple is positioned. The contact coordinate system at each contact point is denoted as b_i , while the coordinate system for the apple is denoted as a_i . The position and orientation of b_i relative to a_i are defined as $w_{abi} = (P_{abi}, R_{abi})$. Consequently, the contact force f_i at each contact point can be represented in the apple coordinate system [18].

$$\begin{bmatrix} R_{abi} & 0 \\ \hat{P}_{abi} R_{abi} & R_{abi} \end{bmatrix} \times B_{bi} \times f_i = G_i f_i \tag{4}$$

Here, \hat{P}_{abi} is expressed as a cross product operator, G_i is the clamping matrix obtained at the contact point i , and B_{bi} is the force spiral base of the contact type with friction point contact.

To stably grasp the apple, the grasping should satisfy the following force balance relationship:

$$GF = \sum_{i=1}^n G_i f_i = -W_{ext} \tag{5}$$

where G represents the grasping matrix at each contact point in the apple coordinate system, F represents the contact force at each contact point in the apple coordinate system, and $-W_{ext}$ represents the external force spiral suffered by the apple. Only by ensuring that the force balance equation has a solution, and the solution is inside the friction cone, can it be explained that the apple grasp is a force-closed grasp.

The judgment condition of the contact force sealing of the end-effector is shown in Figure 2.

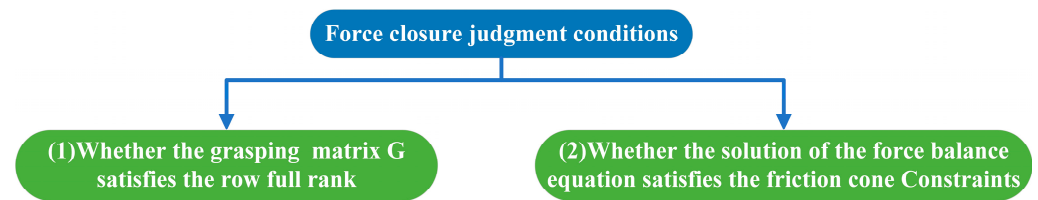


Figure 2. Force closure judgment conditions.

Therefore, combined with the analysis of Sections 2.1 and 2.2, when the end-effector grabs the apple, the three fingers must meet the force closure condition when they are in a balanced state, that is, the contact force spiral and the external force spiral satisfy the force balance relationship shown in Equation (5), and the grasping matrix G row is full rank.

2.3. Torque Constraint and Analysis

The contact force exerted by the fingertip is a result of the joint torque produced by the end-effector. Therefore, a constraint is imposed on the joint torque of the end-effector. This work utilizes the Jacobian matrix to represent the mathematical correlation between the joint torque and the fingertip contact force.

$$J^T f_i = \tau, i = 1, 2 \dots n \tag{6}$$

Here, J is the Jacobian matrix of the end finger, and τ is the joint torque of the end finger.

In summary, in order to ensure that the damage caused by apple picking is as small as possible, the grasping force of the end-effector needs to be optimized under the premise of satisfying the constraints.

To minimize or prevent damage to the fragile and vulnerable apple, it is essential to optimize the contact force applied to it [19].

2.4. Modeling Force Distribution Optimization for End-Effector

As shown in Figure 3, for optimization of the contact force of the end-effector, it is necessary to comprehensively consider the three constraints to ensure the stability of the entire grasping process.

Therefore, the optimization objective can be described as:

$$\begin{aligned}
 &\text{minimize } F_{\max} = \max \|f_{ix}, f_{iy}, f_{iz}\|, i = 1, 2 \dots n \\
 &\text{subject to } \frac{1}{\mu_i} \sqrt{(f_{ix}^2 + f_{iy}^2)} \leq f_{iz}, i = 1, 2 \dots n \\
 &\quad \sum_{i=1}^n G_i f_i = -w_{ext} \\
 &\quad \tau_l \leq J_H^T f_i \leq \tau_r
 \end{aligned} \tag{7}$$

The barrier function is a constraint function. The characteristic of this function is that as the point approaches the feasible region boundary of the optimization problem, its value tends to infinity. The main function deals with the inequality constraint by adding a penalty term to the objective function, so that the optimization problem is easier to deal with. Equation (8) is selected to deal with the inequality constraints in the optimization model from the obstacle function [20] and is used as the penalty term for the optimization goal.

$$k(u) = \begin{cases} 0 & u > 0 \\ \infty & u \leq 0 \end{cases} \tag{8}$$

For the torque constraint, this is processed by a logarithmic barrier function, which can be defined as Equation (9). The domain of the barrier function is $dorm \gamma = \{x \in R^n | g_j(x) \geq 0, j = 1, 2 \dots n\}$. At the same time, $g_j(x) = c_j - d_j^T x$ defines the torque constraint form.

$$\gamma(x) = -\sum_{j=1}^n \ln(g_j(x)) \tag{9}$$

The expression of the torque constraint processed by the obstacle function can be expressed as Equations (10) and (11).

$$\gamma_1(f_i) = -\ln(\tau_r - J_H^T f_i) \tag{10}$$

$$\gamma_2(f_i) = -\ln(-\tau_l + J_H^T f_i) \tag{11}$$

For the friction cone constraint, the constraint is a second-order inequality constraint. A second-order cone is defined in the real range, which satisfies the following conditions:

$$\beta = \left\{ x \in R^{i+1} | \|x_1, x_2 \dots x_i\|_2 \leq \alpha x_{i+1} \right\}, i = 1, 2 \dots n \tag{12}$$

Finally, after processing, the friction cone constraint processing results required in this paper are as follows:

$$\delta(x) = -\ln\left((\mu_i f_{iz})^2 - \|f_{ix}, f_{iy}\|_2^2\right), i = 1, 2 \dots n \tag{13}$$

The optimization challenge for the distribution of contact forces in the end-effector primarily focuses on minimizing the contact force component while satisfying the given constraints. Thus, due to the penalty imposed on the constraint border of the friction cone, the contact force is prevented from approaching the boundary of the friction cone, resulting in a reduction in the magnitude of the joint torque. The construction of the optimization model for the distribution of contact force on the end-effector is demonstrated in Equation (14) [21].

$$\begin{aligned} \omega(f_i, r_k) &= \max \|f_{iz}, f_{ix}, f_{iy}\| - r_k \sum_{u=1}^N \frac{1}{\gamma_u(f_i)} + \frac{1}{\sqrt{r_k}} \sum_{v=1}^M [\delta_v(f_i)^2] \\ &\text{minimize } \omega(f_i, r_k) \\ &\text{subject to } \sum_{i=1}^M G_i f_i = -w_{ext} \end{aligned} \tag{14}$$

Here, r_k represents the penalty factor, N represents the number of end-effector joints, the second part represents the obstacle term, the third is the penalty term, and M represents the number of friction cones in contact. At the same time, the values of r_k and $\frac{1}{\sqrt{r_k}}$ are selected according to the interior point method and the exterior point method, respectively.

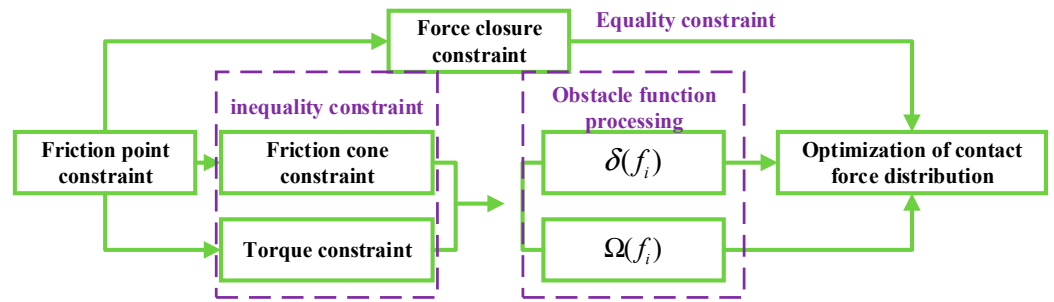


Figure 3. Contact force distribution optimization flow chart.

2.5. Solution to the Contact Force Distribution Optimization Model of End-Effector

The contact force distribution optimization of the three-finger end-effector has been modeled above, and the optimization model will be solved below. The goal of this part is to find the optimal contact force in multiple sets of feasible contact force solutions to minimize the grasping damage on apples. Firstly, the solution set of the force closure constraint condition is decomposed into two parts: the orthogonal special solution f_i^p and the homogeneous solution f_i^h , as shown in Equation (15).

$$f_i = f_i^p + f_i^h = G^+w_{ext} + M\sigma \tag{15}$$

Here, G^+ represents the pseudo-inverse of the grasping matrix G , the matrix M represents the null space of the external force w_{ext} , and σ represents the vector weight of the external force null space w_{ext} . The special solution f_i^p represents the grasping force exerted by the end-effector to balance the external force on the target apple. The homogeneous solution f_i^h represents the grasping internal force exerted by the end-effector under the zero space of the grasping matrix G , and its role is mainly reflected in improving the grasping stability on the apple.

Therefore, the core objective of dynamic force optimization is transformed as shown in Equation (16).

$$\text{minimize } \vartheta(G^+w_{ext} + M\sigma) \tag{16}$$

The quadratic norm defined by the Hessian matrix is used as the step search direction of the Newton iteration algorithm, and the stop criterion of the search is determined by the defined Newton reduction $\sigma + \beta\Delta\sigma_{nt}$ will be iterated as a new predictor for each round:

$$\sigma^* = \sigma + \beta\Delta\sigma_{nt} = \sigma - \beta\nabla^2C(\sigma)^{-1}\nabla C(\sigma) \tag{17}$$

Subsequently, the suitable magnitude of the step β is ascertained using the backtracking line search technique inside the range of (0, 1) to guarantee that each iteration remains within the interval of the viable region [22]. Prior to meeting the search stop requirement, the algorithm will continue searching for a target value that surpasses the current forecast value.

Typically, when the initially chosen feasible solution is far from the desired solution we need to find, the Newton iteration method will require more iterations, and this will significantly decrease computational efficiency. In this part, the solution set of the convex optimization problem exhibits continuity. This means that while the input of σ^* varies smoothly, the output value similarly changes smoothly. Additionally, an estimated solution for the ideal starting value can be obtained [23].

If a feasible initial iteration value cannot be obtained, the specific solution method and steps for the contact force distribution optimization model are shown in Figure 4.

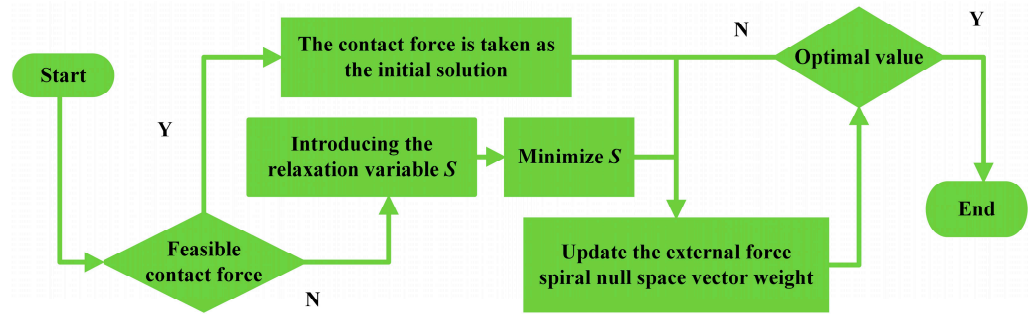


Figure 4. Contact force distribution optimization solution flow chart.

Firstly, a strictly feasible initial solution satisfying the constraint condition of contact force optimization is sought. If there is such a solution, the iterative solution is directly solved. If it does not exist, the relaxation variable S is introduced, and the following optimization description is constructed:

$$\begin{aligned}
 & \text{minimize } s \\
 & \text{subject to } f_i + se \in FH_i, i = 1, 2 \dots n \\
 & \sum_{i=1}^n G_i f_i = -w_{ext} \\
 & \tau_l \leq J_H^T f_i \leq \tau_r
 \end{aligned} \tag{18}$$

where, the relaxation variable $S \in R, S \geq -1$ guarantees that the solution cannot reach negative infinity, $e = (0, 0, 1)$.

In the above second-order optimization problem, the relaxation variable S can be interpreted as a hypothetical force connected to the perpendicular component of the contact force f_i to satisfy the optimization requirements of the grasping issue. The ultimate objective of the optimization problem outlined in Equation (18) is to minimize the virtual force, aiming for a value of 0 or below [21], while ensuring that S is greater than or equal to -1 . If the optimization problem can find a suitable optimal solution, f_i can serve as the initial feasible answer for the original optimization problem related to apple grasping contact force. If the value of the relaxation variable S is consistently greater than 0 in the final solution, it signifies that optimization of the original problem is not possible.

The initial feasible solution in the optimization problem of the relaxation variable S described in Equation (18) can be selected in the following ways. A set of minimum norm solutions satisfying the force closure constraint is taken as the initial contact force f_i :

$$f_i = -G_i^T (G_i G_i^T)^{-1} w_{ext} \tag{19}$$

For the initial relaxation variable S , simply select the value that satisfies the following conditions as its initial value:

$$s > \max \left\{ \frac{1}{\mu_i} \sqrt{(f_{ix}^2 + f_{iy}^2)} \leq f_{iz}, i = 1, 2 \dots n \right\} \tag{20}$$

At this point, the obtained (f_i, s) can be used as the initial feasible solution for the optimization problem of the relaxation variable S constructed using Equation (18).

3. Result and Discussion

3.1. Optimization Example and Simulation of End-Effector Contact Force Distribution

3.1.1. Numerical Example

This section uses MATLAB R2023A to implement the solution for the contact force distribution optimization problem from the previous section. Since only the optimization

solution is verified, and the influence of the penalty factor r_k on the optimization model is not considered, a fixed penalty factor is selected for calculation to verify the feasibility of the optimization solution. Finally, this is compared with the semi-definite programming algorithm in order to obtain better computational efficiency, and optimization of the minimum stable apple grasping force is verified through simulation.

It is assumed that the end-effector is a three-fingered hand, and the apple is grasped according to the position shown in Figure 5. The apple has a uniform centroid in its orthocenter, a mass of 0.3 kg, and a radius of 50 mm. The three-fingered fingertips of the end-effector are in contact with the apple. The positions are $c_1, c_2,$ and c_3 . Zhang et al. [24] conducted a friction measurement experiment, and obtained the friction coefficient. In this paper, the appropriate friction coefficient is selected according to this friction experiment. The friction coefficient is $\mu_i = 0.5$, and the object coordinate system and the contact coordinate system are established at the apple’s center and the contact point, respectively.

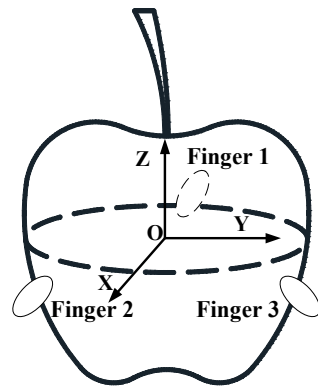


Figure 5. Apple grasping diagram.

The simulation involves using a three-finger end-effector to grip the apple. The specific parameters for this numerical example can be found in Table 1. The contact point coordinates specify the location of the three fingers in relation to the coordinate system of the object.

Table 1. Contact point parameters of the end-effector.

Finger Number	X	Y	Z
1	−48.51	0	−12.26
2	22.45	−41.25	−12.26
3	22.45	41.25	−12.26

Since the coordinates of the contact points are the representation of the contact points in the object coordinate system, the pose of the contact coordinate system relative to the object coordinate system can be calculated according to the coordinates of the contact points, and the grasping matrix G_i of the three fingers can be obtained. The complete grasping matrix G can be obtained by combining them:

$$G = \begin{bmatrix} 0 & 1 & 0 & 1 & 0 & 0 & 1 & 0 & 0 \\ -0.5929 & 0 & 0.7914 & 0 & -0.8137 & -0.5812 & 0 & 0.8137 & -0.5812 \\ -0.7914 & 0 & 0.5929 & 0 & 0.5812 & 0.8137 & 0 & 0.5812 & 0.8137 \\ -7.2689 & 0 & 9.7026 & 0 & -33.9504 & -40.6906 & 0 & 33.9504 & 26.4396 \\ -33.6424 & -12.26 & 25.2042 & -12.26 & -13.0749 & -18.2672 & -12.26 & -13.0749 & -18.2672 \\ 25.2042 & 0 & -33.6424 & 41.25 & -18.2672 & -13.0749 & -41.25 & 18.2672 & -13.0749 \end{bmatrix}$$

The contact force vector is:

$$f = [f_{1,x}, f_{1,y}, f_{1,z}, f_{2,x}, f_{2,y}, f_{2,z}, f_{3,x}, f_{3,y}, f_{3,z}] \tag{21}$$

The friction cone constraint is:

$$FH = FH_1 \times FH_2 \times FH_3 \tag{22}$$

$$FH_i = \left\{ f_i \in R^3 \mid \frac{1}{\mu_i} \sqrt{(f_{ix}^2 + f_{iy}^2)} \leq f_{iz}, i = 1, 2, 3 \right\} \tag{23}$$

The Jacobian matrix of the end-effector fingertips is:

$$J_H = \begin{bmatrix} 0 & 54.276 & 102.244 & 0 & 0 & 0 & 0 & 0 & 0 \\ 0 & -6.283 & 83.584 & 0 & 0 & 0 & 0 & 0 & 0 \\ 0 & 0 & 0 & -61.576 & 0 & 114.012 & 0 & 0 & 0 \\ 0 & 0 & 0 & 13.014 & 0 & -96.376 & 0 & 0 & 0 \\ 0 & 0 & 0 & 0 & 0 & 0 & -61.576 & 0 & 114.012 \\ 0 & 0 & 0 & 0 & 0 & 0 & -13.014 & 0 & 96.376 \end{bmatrix}$$

Each joint torque of the end-effector is $\tau_l = -3 \text{ N}\cdot\text{m}$, $\tau_r = 3 \text{ N}\cdot\text{m}$. According to the selected penalty factor $r_k = 4$, a set of optimal contact forces is obtained:

$$f = [2.483, 1.679, 4.073, 1.779, 1.613, 2.048, 2.569, 1.463, 3.164]^T$$

Applying the semi-definite programming approach to determine the ideal contact force in the given gripping scenario will need additional floating-point operations, resulting in a significant decrease in computational efficiency. The precise calculation efficiency is displayed in Table 2, and these are compared in the same context of a computer with the Windows 11 operating system and MATLAB R2023A (9.14.0.2206163) 64-bit (win64) software.

Table 2. Computational efficiency comparison index.

Contrast Ratio	Method of this Article	Semidefinite Programming Algorithm
Computing time (ms)	0.346	0.675
Number of convergences	5	9
Number of floating-point operations (kflops)	7	19

3.1.2. Grasping Simulation

The previous section verified the efficiency of the improved Newton iterative algorithm in solving the optimization problem of contact force distribution under fixed penalty factors. This section will continue to study the selection of penalty factors in MATLAB R2023A by selecting appropriate penalty factors for the entire optimization model of contact force distribution, simulating the three-finger grasp and observing the law of contact force change.

In the simulation process, the apple object coordinate system is always kept at the position of $p = (0, -4, 2.5)$ relative to the end-effector coordinate system. At this time, the contact position and vector of each end-effector fingertip are:

$$R_{oc1} = [0.87, 0, 0.5] \quad R_{oc2} = [-0.8, 0.5, 0] \quad R_{oc3} = [0.8, 0.5, 0]$$

$$p_{oc1} = [0.87, 15, -2.5] \quad p_{oc2} = [13, 7.5, 4.35] \quad p_{oc3} = [-14, 7.5, 4.35]$$

The penalty factor r_k is gradually increased from 0.1 to 100 with a step size of 0.1, and the optimal contact force normal component f_{iz} of each finger is recorded in turn. The variation of the normal contact force f_{iz} with the penalty factor r_k is shown in Figure 6. By observing the change rule of the following figure, it can be expected that when the penalty factor r_k gradually increases, the contact force of the end-effector's three fingertips will be significantly reduced, and this will also increase the possibility of grasping failure.

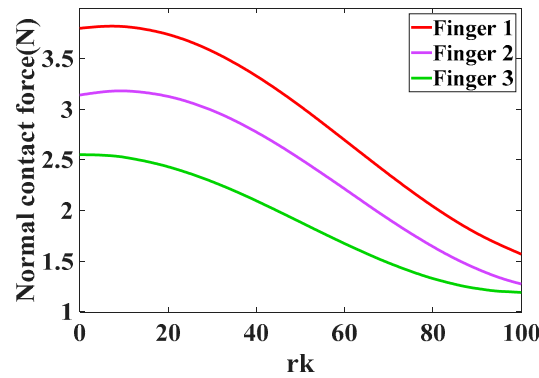


Figure 6. Contact force variation diagram.

To establish a well-defined boundary for the penalty factor r_k , the friction residual and the torque residual are introduced. These residuals serve as approximations to assess the proximity of the constraint boundary of the friction cone and the difference between the joint torque and the limit torque of each finger, respectively. The torque residual and friction residual, which are normalized, are depicted in Figure 7, showcasing their variation with the penalty factor r_k as indicated in Equations (24) and (25).

$$\varphi_\tau = \text{minimize } \{|\tau_i - \tau_{lim}|\}, i = 1, 2, 3 \tag{24}$$

$$\varphi_F = \text{minimize } \left\{ \mu_i f_{iz} - \|f_{ix}, f_{iy}\|_2 \right\}, i = 1, 2, 3 \tag{25}$$

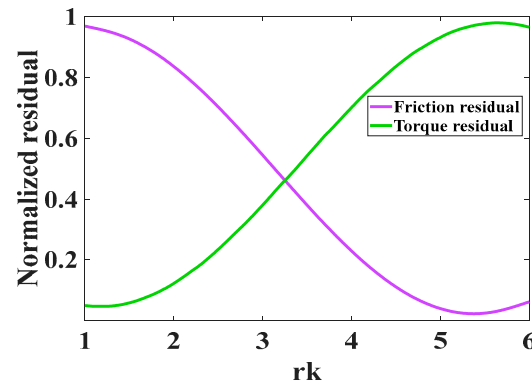


Figure 7. Residual variation diagram.

It can be seen from the Figure 7 that when r_k is large, the penalty for the joint torque is more severe, and the joint torque is small. At this time, there is a risk of grasping failure. When r_k is small, the penalty near the edge of the friction cone is more severe. At this time, the torque is larger and the grasp is more stable. Therefore, when the friction residual φ_F is equal to the torque residual φ_τ , the penalty factor value is the best trade-off between improving grasping stability and reducing apple damage.

The selected penalty factor $r_k = 3.25$ is substituted into the contact force optimization model for grasp simulation. The gravity center of the apple is still maintained at the position relative to the end-effector coordinate system $p = (0, -4, 2.5)$. The movement time of the simulation is 3 s. The law of the contact force generated by the three fingertips over time and the torque residuals are shown in Figures 8 and 9. From the diagram, it can be observed that the contact force component generated by the three fingertips does not exceed the torque limit value. This shows that during the whole simulated grasping process, the three fingers never slide, and the grasping is stable. Finally, the whole simulation proves that the contact force distribution optimization scheme proposed in this study is feasible.

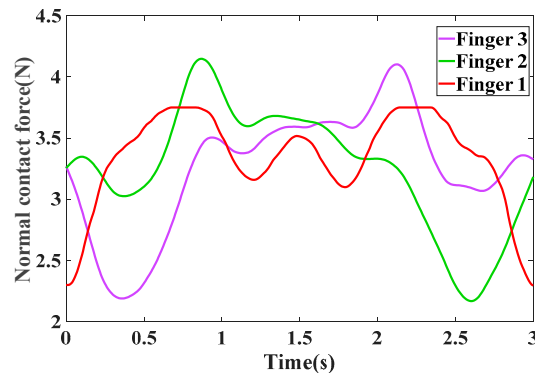


Figure 8. Contact force variation law.

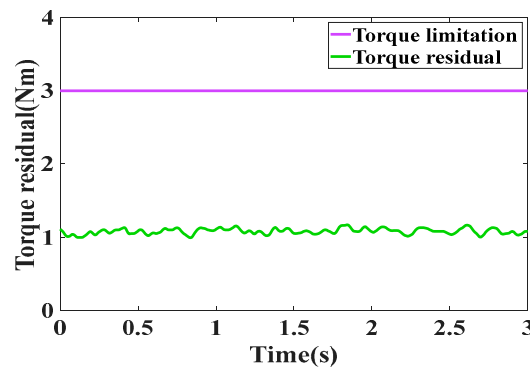


Figure 9. Torque residual.

The optimal contact force of the apple picking robot end-effector developed in the laboratory is solved by the contact force optimization scheme proposed in this section. Finally, a set of solutions are obtained as follows:

$$f = [4.597, 3.648, 5.152, 4.779, 3.793, 5.178]^T$$

3.2. Contact Force Distribution Optimization Experiment of End-Effector

3.2.1. Experimental Equipment

The apple picking robot is shown in Figure 10a, which consists of a chassis, a robot arm, an end-effector, a camera, and a controller. The experimental equipment will be used to verify the optimization of grasping force in practical experiments.

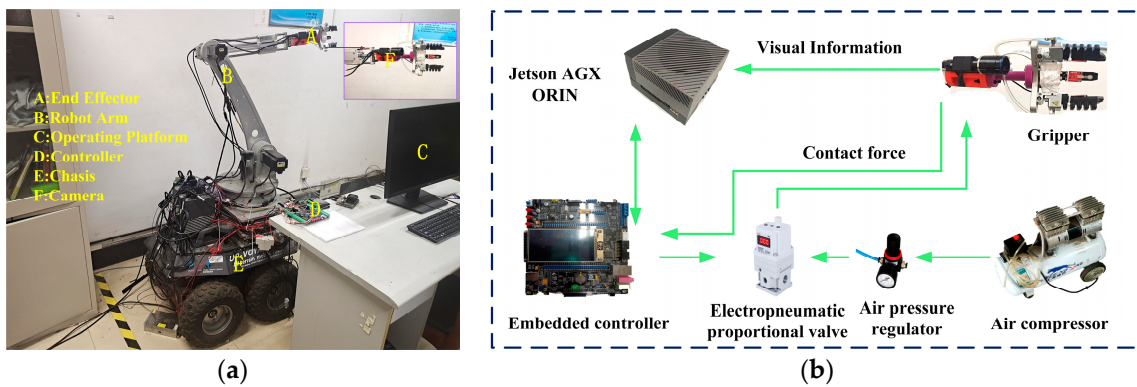


Figure 10. The experimental equipment. (a) Apple picking robot; (b) the control system diagram of the end-effector.

The control system diagram of the end-effector is shown in Figure 10b, which consists of an end-effector, a Jetson AGX ORIN, an embedded controller, a force sensor, a cylinder,

and an electric proportional valve. The end-effector is mounted on a Festo push rod for picking apples. During the grasping task, the grasping force signal between the end-effector and the apple is detected by the force sensor and transmitted to the embedded controller. The embedded controller adjusts the electric proportional valve according to the error to achieve force control. Finally, it determines whether the apple slips or the grasping is successful based on whether there is a sudden change in the grasping force.

3.2.2. Grasping Experiment and Analysis

The numerical samples and simulation verify the practicality of the contact force optimization approach when grasping apples. Nevertheless, throughout grasping, it is possible for the position of contact and the friction coefficient to undergo alterations. These changes can be specified to follow a normal distribution with a change rate of 0.05. The following equation can be employed to define the threshold of grasping stability:

$$s = \underset{i=1,2}{\text{minimize}} \|f_{ix}, f_{iy}, f_{iz}\| - \underset{i=1,2}{\text{optimize}} \|f_{ix}, f_{iy}, f_{iz}\| \tag{26}$$

where, $\underset{i=1,2}{\text{minimize}} \|f_{ix}, f_{iy}, f_{iz}\|$ represents the minimum grasping force required to satisfy the grasping stability condition in the actual grasping process, and $\underset{i=1,2}{\text{optimize}} \|f_{ix}, f_{iy}, f_{iz}\|$ represents the optimal grasping force obtained by the contact force distribution optimization algorithm. When $S < 0$, it indicates that there is an unmet constraint condition for grasping failure, otherwise it means that the grasp is successful.

Figure 11 shows the success rate results obtained by 1000 Monte Carlo simulation probability analysis iterations for each penalty factor under different penalty factors. If the above-mentioned conditions for successful grasping are met, it is recorded as Y , otherwise it is recorded as N . Until the end of the iteration, the number of successful grasps is T_Y , and the number of failed grasps is T_N , so the success rate of grasping can be calculated as:

$$P_Y = T_Y / (T_N + T_Y) \tag{27}$$

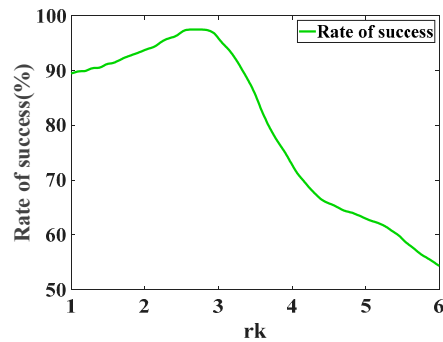


Figure 11. Curve of grasp success rate.

It can be observed from the above figure that when the penalty factor is in the range of (1, 3.3), the grasping success rate is higher, basically above 90%, and the contact force distribution optimization scheme proposed in this paper also shows high stability. When the value of r_k exceeds this interval, the probability of sliding during the actual grasping process will increase. An r_k value in the interval of (1, 3.3) and outside this interval are simulated several times.

In the actual experiment, a red Fuji apple was used as the grasping object for grasping verification. The red Fuji apple peel was smooth, shiny, medium thick, tough, and waxy. The relatively stable apple grasp results and the sliding grasp results can be observed, as shown in Figure 12a,b.

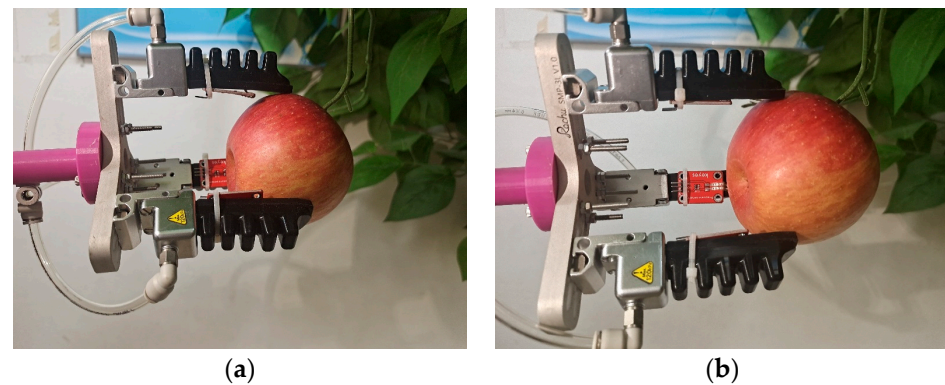


Figure 12. Comparison of grasping phenomena with different penalty factors. (a) Stable grasp; (b) sliding grasp.

The aforementioned studies demonstrate that selecting the penalty factor within the range of (1, 3.3) results in the best success rate for grasping, hence confirming the reliability of the contact force optimization model. To calculate the lowest stable grasping force input for the end-effector controller, we will monitor the damping control variable [25] to detect any sudden changes in the real grabbing force, which may indicate whether the apple is sliding. Figure 13 displays the experimental results of the grasping force distribution with different penalty factors.

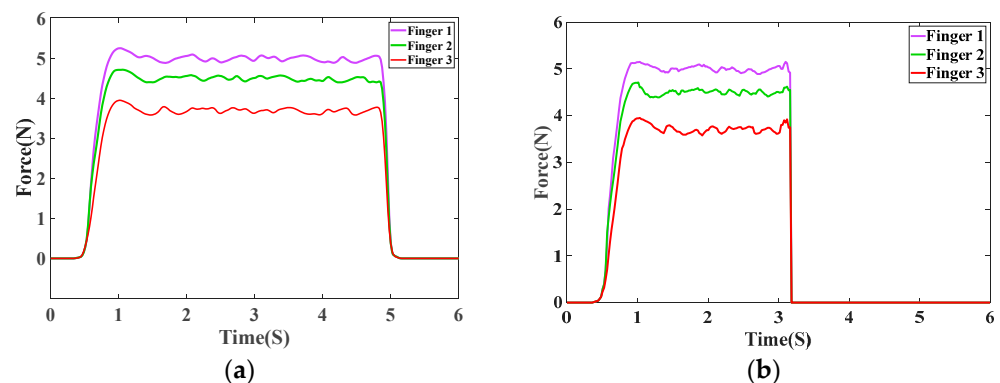


Figure 13. Experimental results of the grasping force distribution with different penalty factors. (a) Stable grasp; (b) sliding grasp.

The experimental results show that there is no sudden change in contact force during the grasping process, that is, the apple does not slide. When the penalty factor is selected within the range of (1, 3.3), the optimal contact force solved by the contact force optimization model can result in stable grasping.

3.3. Discussion

In this study, the grasp stability of end-effectors was analyzed based on the force closure theory, the constraint conditions were treated using an obstacle function, and an optimal model of end-effector contact force distribution was constructed by introducing penalty factors. Then, the improved Newton method was used to solve the contact force distribution model. The optimal contact force for grasping apples was determined using numerical case simulation analysis on the premise of selecting the penalty factor, and the effectiveness of the solution was verified. Finally, the practical significance of the method for apple grasping is verified in an actual grasping experiment. The experiment showed that the method can provide the minimum stable grasping force for the end-effector to achieve a stable grasp, and avoid sliding caused by a too small grasp force or fruit damage caused by a too large grasp force. Although this method realizes a stable grasp of the apple, the computational cost still exists. In many special weather conditions such as rain, dew or

high humidity, apples have less friction, which has not been studied. This would require a lot of programming. The development of soft manipulator claws or slip detection are good research directions, which could also achieve the lossless and stable grasp of apples. In the future, we will study the sliding friction and sliding signal detection of an apple grasp.

4. Conclusions

In this paper, the grasping stability of end-effectors was analyzed based on the force closure theory, considering the force closure constraint, the nonlinear friction cone constraint and the torque. The constraint conditions were processed using an obstacle function, and the contact force distribution optimization model of a three-finger end-effector was constructed by introducing a penalty factor. The improved Newton method was used to solve the contact force distribution model, and through numerical simulation analysis, it was found that the optimal contact force for grasping a target apple can be determined under the premise of selecting the penalty factor. The calculation efficiency was compared with that of the semi-definite programming algorithm. It was found that the calculation time of the method proposed in this paper was 0.346 ms, while the semi-definite cost-effective rule required 0.675 ms, which verified the efficiency of the proposed method. It was found that the optimal contact force solved by the optimization method did not exceed the torque limit by using MATLAB simulation. The iterative method of Monte Carlo simulation probability analysis was used to calculate the optimal contact force required for grasping stability under different penalty factors for multiple iterations. It was found that when the penalty factor was selected within the range [1,3.3], the grasping success rate was the highest, basically reaching more than 90%. The actual grasping experiment further verified that this method can provide the minimum stable grasping force needed for the apple picking robot and achieve the stable grasping of apples. Based on the results of this experiment, we will consider comparing research on the friction force and friction coefficient of an apple under wet and dry conditions in the future, and further study the compliance control strategy based on sliding signal analysis.

Author Contributions: Conceptualization, W.J. and H.Z.; methodology, B.X. and H.Z.; software, H.Z. and X.Y.; validation, X.Y.; formal analysis, H.Z.; investigation, W.J.; data curation, H.Z.; resources, W.J.; writing—original draft preparation, H.Z.; writing—review and editing, W.J. and X.Y.; visualization, B.X.; supervision, W.J.; project administration, W.J.; funding acquisition, B.X. and W.J. All authors have read and agreed to the published version of the manuscript.

Funding: This research was funded by the National Natural Science Foundation of China (No. 61973141) and a project funded by the Priority Academic Program Development of Jiangsu Higher Education Institutions (No. PAPD).

Institutional Review Board Statement: Not applicable.

Data Availability Statement: Data are contained within the article.

Conflicts of Interest: The authors declare no conflicts of interest.

References

1. Zhang, K.; Lammers, K.; Chu, P.; Li, Z.; Lu, R. System design and control of an apple harvesting robot. *Mechatronics* **2021**, *79*, 102644. [[CrossRef](#)]
2. Ji, W.; He, G.; Xu, B.; Zhang, H.; Yu, X. A new picking pattern of a flexible three-fingered end-effector for apple harvesting robot. *Agriculture* **2024**, *14*, 102. [[CrossRef](#)]
3. Gongal, A.; Amatya, S.; Karkee, M.; Zhang, Q.; Lewis, K. Sensors and systems for fruit detection and localization: A review. *Comput. Electron. Agric.* **2015**, *116*, 8–19. [[CrossRef](#)]
4. Chen, Z.; Wu, Q.; Hong, C.; Zhang, X. Multi-fingered grasping force optimization based on generalized penalty-function concepts. *Robot. Auton. Syst.* **2021**, *135*, 103672. [[CrossRef](#)]
5. James, J.; Lepora, N. Slip detection for grasp stabilization with a multi-fingered tactile robot hand. *IEEE Trans. Robot.* **2021**, *37*, 506–519. [[CrossRef](#)]
6. Mavrakis, N.; Hao, Z.; Gao, Y. On-orbit robotic grasping of a spent rocket stage: Grasp stability analysis and experimental results. *Front. Robot. AI* **2021**, *8*, 652681. [[CrossRef](#)]

7. Xu, W.; Guo, W.; Shi, X.; Sheng, X.; Zhu, X. Fast force-closure grasp synthesis with learning-based sampling. *IEEE Robot. Autom. Lett.* **2023**, *8*, 4275–4282. [[CrossRef](#)]
8. Li, Z.; Li, P.; Yang, H.; Wang, Y. Stability tests of two-finger tomato grasping for harvesting robots. *Biosyst. Eng.* **2013**, *116*, 163–170. [[CrossRef](#)]
9. Buss, M.; Hashimoto, H. Dextrous hand grasping force optimization. *IEEE Trans. Robot. Autom.* **1996**, *12*, 406–418. [[CrossRef](#)]
10. Li, Q.; Gao, D.; Deng, H. The sealing of the contact force of the heavy-duty clamping device. *J. Mech. Eng. Sci.* **2010**, *46*, 36–42. [[CrossRef](#)]
11. Liang, Z.; Jiang, B.; Quan, P.; Lin, H.; Lou, Y.; Di, S. Force-closure analysis of multilink cable-driven redundant manipulators considering cable coupling and friction effects. *IEEE-ASME Trans. Mechatron.* **2023**, *in press*. [[CrossRef](#)]
12. Liu, Z.; Jiang, L.; Yang, B. Task-oriented real-time optimization method of dynamic force distribution for multi-fingered grasping. *Int. J. Humanoid Robot.* **2022**, *19*, 2250013. [[CrossRef](#)]
13. Li, G.; Xu, P.; Qiao, S.; Li, B. Stability analysis and optimal enveloping grasp planning of a deployable robotic hand. *Mech. Mach. Theory* **2021**, *158*, 104241. [[CrossRef](#)]
14. Liu, Q.; Xu, Y.; Zhou, Y. A class of exact penalty functions and penalty algorithms for non-smooth constrained optimization problems. *J. Glob. Optim.* **2020**, *76*, 745–768. [[CrossRef](#)]
15. Liu, Y.; Jiang, D.; Tao, B.; Qi, J.; Jiang, G.; Yun, J.; Huang, L.; Tong, X.; Chen, B.; Li, G. Grasping posture of humanoid manipulator based on target shape analysis and force closure. *Alex. Eng. J.* **2022**, *61*, 3959–3969. [[CrossRef](#)]
16. Dharbaneshwer, S.; Thondiyath, A. Contact area-based modeling of robotic grasps using deformable solid mechanics. *Int. J. Appl. Mech.* **2021**, *13*, 2150038. [[CrossRef](#)]
17. Benkhira, E.; Fakhar, R.; Mandly, Y. Analysis and numerical approximation of a contact problem involving nonlinear hencky-type materials with nonlocal coulomb's friction law. *Numer. Funct. Anal. Optim.* **2019**, *40*, 1291–1314. [[CrossRef](#)]
18. Wang, Y.; Dehio, N.; Kheddar, A. On inverse inertia matrix and contact-force model for robotic manipulators at normal impacts. *IEEE Robot. Autom. Lett.* **2022**, *7*, 3648–3655. [[CrossRef](#)]
19. Righetti, L.; Buchli, J.; Mistry, M.; Kalakrishnan, M.; Schaal, S. Optimal distribution of contact forces with inverse-dynamics control. *Int. J. Robot. Res.* **2013**, *32*, 280–298. [[CrossRef](#)]
20. Liu, J. Converse barrier functions via Lyapunov functions. *IEEE Trans. Autom. Control* **2022**, *67*, 497–503. [[CrossRef](#)]
21. Deng, Z.; Fang, B.; He, B.; Zhang, J. An adaptive planning framework for dexterous robotic grasping with grasp type detection. *Robot. Auton. Syst.* **2021**, *140*, 103727. [[CrossRef](#)]
22. Chen, Y.; Sun, Q.; Guo, Q.; Gong, Y. Dynamic modeling and experimental validation of a water hydraulic soft manipulator based on an improved newton-euler iterative method. *Micromachines* **2022**, *13*, 130. [[CrossRef](#)] [[PubMed](#)]
23. Agrawal, A.; Barratt, S.; Boyd, S. Learning convex optimization models. *IEEE-CAA J. Autom. Sin.* **2021**, *8*, 1355. [[CrossRef](#)]
24. Zhang, X.; Yin, L.; Shang, S.; Chung, S. Mechanical properties and microstructure of Fuji apple peel and pulp. *Int. J. Food Prop.* **2022**, *25*, 1773–1791. [[CrossRef](#)]
25. Ji, W.; Tang, C.; Xu, B.; He, G. Contact force modeling and variable damping impedance control of apple harvesting robot. *Comput. Electron. Agric.* **2022**, *198*, 107026. [[CrossRef](#)]

Disclaimer/Publisher's Note: The statements, opinions and data contained in all publications are solely those of the individual author(s) and contributor(s) and not of MDPI and/or the editor(s). MDPI and/or the editor(s) disclaim responsibility for any injury to people or property resulting from any ideas, methods, instructions or products referred to in the content.